Ubiquity of ring structures in the control space of complex oscillators

Cite as: Chaos **31**, 101102 (2021); https://doi.org/10.1063/5.0066877
Submitted: 12 August 2021 . Accepted: 17 September 2021 . Published Online: 04 October 2021

Gonzalo Marcelo Ramírez-Ávila, Jürgen Kurths and Jason A. C. Gallas

Chaos ARTICLE scitation.org/journal/cha

Ubiquity of ring structures in the control space of complex oscillators

Cite as: Chaos **31**, 101102 (2021); doi: 10.1063/5.0066877
Submitted: 12 August 2021 · Accepted: 17 September 2021 ·
Published Online: 4 October 2021

Gonzalo Marcelo Ramírez-Ávila,[1,2,3] Jürgen Kurths,[3,4,5] and Jason A. C. Gallas[1,2,6,a)]

AFFILIATIONS

[1]Instituto de Investigaciones Físicas, Universidad Mayor de San Andrés, La Paz, Bolivia
[2]Instituto de Altos Estudos da Paraí ba, Rua Silvino Lopes 419-2502, 58039-190 João Pessoa, Brazil
[3]Potsdam Institut für Klimafolgenforschung, 14412 Potsdam, Germany
[4]Institut für Physik, Humboldt-Universität zu Berlin, 10115 Berlin, Germany
[5]Lobachevsky University of Nizhny Novgorod, Nizhnij Novgorod 603950, Russia
[6]Complexity Sciences Center, 9225 Collins Avenue Suite 1208, Surfside, Florida 33154, USA

[a)]**Author to whom correspondence should be addressed:** jason.gallas@gmail.com

ABSTRACT

We report the discovery of two types of *stability rings* in the control parameter space of a vertical-cavity surface-emitting semiconductor laser. Stability rings are closed parameter paths in the laser control space. Inside such rings, laser stability thrives even in the presence of small parameter fluctuations. Stability rings were also found in rather distinct contexts, namely, in the way that cancerous, normal, and effector cells interact under ionizing radiation and in oscillations of an electronic circuit with a junction-gate field-effect transistor (JFET) diode. We argue that stability-enhancing rings are generic structures present in the control parameter space of many complex systems.

Recently, high-performance computer clusters combined with reliable numerical methods have been revealing a plethora of intricate structures in stability diagrams of several complex nonlinear oscillators. This paper reports two types of stability rings observed in three rather unalike dynamical systems, namely, in the control parameter space of a state-of-the-art model of a vertical-cavity surface-emitting semiconductor laser, in a model of the dynamics of cancerous cells subjected to ionizing radiation, and in the inductor-based Hartley electronic circuit with a JFET and the usual tapped coil. Here, selected control parameter planes of these three complex oscillators are shown to display rings, i.e., closed parameter paths, formed by periodic oscillations along which the number of spikes per period remains constant or not. The existence of such stability rings cannot be predicted theoretically due to the total absence of an adequate framework to solve analytically coupled nonlinear differential equations. However, stability rings should not be difficult to validate experimentally. We believe stability rings to be generic structures present in the control parameter space of many other complex systems underlying important applications.

I. INTRODUCTION

A key aspect of lasers design and optimization is the definition of their operational control parameters. In general, design and optimization are hard to perform experimentally because of the need for searching adequate lasing conditions by tuning several material properties simultaneously over wide parameter ranges, as well as laser cavity geometry.[1–3] However, high-performance and high-throughput computer clusters offer an efficient alternative to explore wide parameter ranges of interest. Such clusters allow extended numerical simulations, thanks to the availability of well tested and reliable numerical methods. Numerical simulations are considerably less expensive alternatives that are more time-effective than systematic and arduous experimental laboratory searches for suitable material properties.

This paper reports remarkable structures, namely, two types of stability rings, observed in the control parameter space of a vertical-cavity surface-emitting semiconductor laser (VCSEL). As illustrated by Figs. 1, 2, 3, stability rings are closed parameter paths, loops in the control space, characterized by periodic oscillations. Along closed paths, oscillations display a constant number of spikes per period

and are monocolored circuits like any of the paths in Fig. 1. Alternatively, loops may display multicolored segments, like in Fig. 3(c), signaling that the number of spikes is not constant along the closed path. Apart from their theoretical novelty, such rings are particularly interesting because, as described below, laser stability thrives inside such rings, even in the presence of small parameter fluctuations.

We have also been able to detect similar stability rings in rather distinct complex systems and, therefore, believe that they might be common features of a large class of nonlinear oscillators. In addition to the semiconductor laser, here we also report stability rings detected in a realistic model, based on clinical data,[4] describing the dynamics of cancerous cells[5] and to which the effect of ionizing radiation was included[6–11] and in a JFET-based electronic circuit used in modern communication systems.[12,13]

We begin by describing in detail the stability rings found for the VCSEL. We then corroborate the properties described for the VCSEL rings in both aforementioned examples. These additional examples are just intended to show that rings are not *fragile* or hard to find in other typical nonlinear dynamical systems.

II. RINGS IN A SEMICONDUCTOR LASER

A VCSEL has several advantages over edge-emitting lasers and this is the reason for the many recent experimental[14,15] and theoretical studies[16,17] about them. For instance, Refs. 14–17 reported on the interplay between polarization switching and bifurcations in VCSELs when subjected to orthogonal optical injection. They found qualitatively different bifurcation scenarios leading to polarization switching in the plane of the injection parameters, namely, the frequency detuning and injection strength plane. A Hopf bifurcation mechanism on the two-polarization-mode solution determines the injection-locking boundaries and influences polarization switching induced by optical injection. A torus bifurcation emerging from a two linearly polarized (LP) mode time-periodic dynamics was reported to arise before polarization switching and injection locking appear. This corresponds to an interesting combination of relaxation oscillation dynamics in the x-LP mode together with wave mixing dynamics in the injected y-LP mode. In agreement with experiments, Gatare *et al.*[14–16] described a period-doubling route to chaos that involves both VCSEL orthogonal LP modes.

All aforementioned remarkable features motivated us to perform a detailed investigation on the VCSEL state-of-the-art model considered in Ref. 16, namely,

$$\frac{dE_x}{dt} = \kappa(1+i\alpha)(NE_x + inE_y - E_x) - i(\gamma_p + \Delta\omega)E_x - \gamma_a E_x, \quad (1)$$

$$\frac{dE_y}{dt} = \kappa(1+i\alpha)(NE_y - inE_x - E_y) + i(\gamma_p - \Delta\omega)E_y + \gamma_a E_y + \kappa_{inj}E_{inj}, \quad (2)$$

$$\frac{dN}{dt} = -\gamma_e(1+A)N + \gamma_e\mu - i\gamma_e Bn, \quad (3)$$

$$\frac{dn}{dt} = -\gamma_s n - \gamma_e An - i\gamma_e BN, \quad (4)$$

where $A = |E_x|^2 + |E_y|^2$, $B = E_yE_x^* - E_xE_y^*$, and E_x and E_y represent the slowly varying components of the linearly polarized electric fields in, respectively, the x- and y-polarization directions. The variable N accounts for the total population inversion between conduction and valence bands, while n accounts for the difference in the carrier numbers of the two sublevels with opposite spins.

The parameters are defined as follows: κ is the optical field decay rate, γ_e is the decay rate of N, γ_s is the spin-flip relaxation rate, γ_α the linear dichroism, γ_p the linear birefringence, α is the usual linewidth enhancement factor, and μ is the normalized injection current ($\mu = 1$ at threshold). An external optical injection is modeled through the coupling coefficient κ_{inj}, the injected field amplitude E_{inj}, and $\Delta\omega$ which accounts for the frequency detuning between master average and slave frequencies. The free-running laser may exhibit two frequencies, which correspond to the frequencies of the two linearly polarized modes. In the stationary case, the frequencies of the two LP modes are given by $\omega_{x,y} = \mp\gamma_p \pm \alpha\gamma_\alpha$. The frequency detuning is the detuning between the master frequency ω_{inj} and a frequency ω_{th} intermediate between that of the x- and the y-LP modes $\omega_{\text{th}} = (\omega_x + \omega_y)/2$, i.e., $\Delta\omega = \omega_{\text{inj}} - \omega_{\text{th}}$. The intensities in x- and y-directions are $I_{x,y} = |E_{x,y}|^2$. In agreement with experiments,[14–17] we fix $\kappa = 300 \times 10^9$, $\gamma_p = 30 \times 10^9$, $\gamma_a = 0.5 \times 10^9$, $\gamma_e = 1.0 \times 10^9$, $\gamma_s = 50 \times 10^9$, $\alpha_e = 3.0$, $\mu = 1.5$, and $\kappa_{\text{inj}} = 300 \times 10^9$ and study mode spiking as a function of the injected field amplitude E_{inj} and detuning $\Delta\omega$.

We computed two types of stability diagrams: the standard Lyapunov diagrams[18] and the so-called *isospike* diagrams.[19–29] Here, isospike diagrams are constructed by painting each point of the control plane with colors reflecting the number of spikes (local maxima) per period of the periodic oscillations and assigning some specific color to record nonperiodic oscillations. Computationally, isospike diagrams are a much simpler and less costly way to obtain all the information of Lyapunov diagrams, plus a significant enhancement: instead of lumping together all periodic oscillations into a single-phase as Lyapunov diagrams do, isospike diagrams classify oscillations by explicitly displaying the number of spikes per period for every individual oscillation. For a survey on the computation of stability diagrams, see Ref. 22. Figures 1–3 are examples of isospike diagrams. Their chaotic phases were corroborated by computing the magnitude of the Lyapunov exponents (not shown).

Each panel in Fig. 1 was obtained by solving the equations of motion, Eqs. (1)–(4), on a grid of $2400 \times 2400 = 5.76 \times 10^6$ equally spaced points with the standard fourth-order Runge–Kutta integrator with fixed-step $h = 10^{-12}$. For each grid point, periodicities were determined by inspecting the behavior of 4×10^6 timesteps after discarding a transient of 2×10^6 steps. Integrations were started from arbitrarily selected initial conditions, viz., $E_{x\parallel}(0) = 0.2$, $E_{x\perp}(0) = 0.4$, $E_{y\parallel}(0) = 0.3$, $E_{y\perp}(0) = 0.6$, $N(0) = 1.05$, and $n(0) = 0.05$. However, our results are relatively insensitive to the initial conditions used.

Figure 1 shows isospike diagrams for the VCSEL, obtained by counting spikes per period of $E_{y\parallel}$, the interesting component of the electric field parallel to the polarization direction. In Fig. 1(a), it is not difficult to recognize two types of closed circuits or rings: two larger rings involving multiple circuits characterized by regular laser modes with 12 and 16 spikes per period, and a smaller ring formed by regular oscillations with 20 spikes per period, shown magnified in

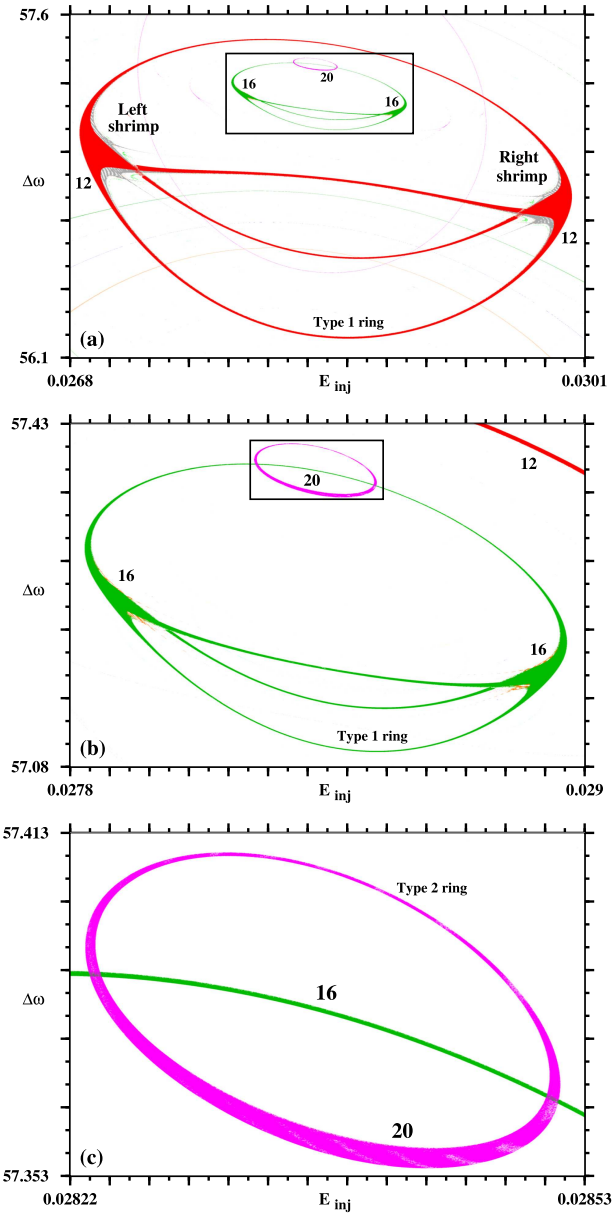

FIG. 1. Isospike diagrams showing stable structures for the VCSEL, illustrating the two types of rings observed in the injected field amplitude E_{inj} vs the frequency detuning $\Delta\omega$ control space. Numbers refer to the number of spikes per period of $E_{y\|}$. The white background marks parameters leading to nonperiodic (chaotic) oscillations. Type-1 rings with three circuits in (a) and (b) involve two shrimps,[30–35] while the type-2 ring in (c) does not. Panels (b) and (c) are magnifications of details in panel (a). See the text.

Figs. 1(b) and 1(c). Rings with multiple circuits are formed by interconnecting two *shrimps*[30–35] while the single circuit ring in Fig. 1(c) involves no shrimps. Shrimps are complex structures with four main legs displaying infinite successions of spike-doubling cascades of periodic oscillations in addition to the chaotic phases that follow them.[22,30–35] The presence or not of shrimps allows one to distinguish both types of rings. The regular ring sequence, as well as the regular spikes proliferation of the rings, in Fig. 1 seem to suggest that the type-2 ring in Fig. 1(c) could arise from a shrimp "annihilation" process in which the multiple shrimp legs of the type-1 rings get closer and closer until they eventually vanish, with the ring becoming a type-2 ring. Next, we describe stability rings found in the cancer model.

III. RINGS IN CANCEROUS CELLS MODEL

As a second example of a complex oscillator, we consider a tumor growth model based on clinical data describing the dynamics among cancerous, normal, and effector cell populations,[4,5] subjected to ionizing radiation acting on both malignant and normal cells.[6–11] The model considered here is governed by the following nonlinearly coupled equations:

$$\begin{aligned}\frac{dT}{dt} &= T(1-T) - aTN - bTI - rT,\\ \frac{dN}{dt} &= cN(1-N) - dTN - rN,\\ \frac{dI}{dt} &= \frac{\varepsilon IT}{T+f} - gIT - hI,\end{aligned} \tag{5}$$

where T, N, and I represent the tumor, normal, and effector cells populations, respectively. The parameter r controls the applied radiation, which inhibits both cancerous and healthy cells. The other parameters are related to the growth rates and the excitatory and inhibitory interactions among the different cells.[4,10,11] Here, we fix the realistic values $a = 1.0$, $b = 2.5$, $c = 0.6$, $\varepsilon = 4.5$, $f = 1.0$, $h = 0.5$, and $r = 10^{-3}$ and arbitrarily selected initial conditions $(T, N, I) = (0.69, 0.30, 0.01)$, but are relatively insensitive to changes. Integrations are done as before, with a timestep $\Delta t = 0.05$, disregarding the first 6×10^6 steps as transient, and subsequently using an equal amount of steps to determine the number of spikes.

Figure 2 shows a sequence of isospike stability diagrams for the cancer model with radiation, Eq. (5), obtained by counting spikes per period in the normal cells population. Figure 2(a) shows a global view of the parameter space and a box locating a region of interest here, shown magnified in Fig. 2(b). The pair of boxes in Fig. 2(b) are magnified in Figs. 2(c) and 2(d), which contain type-1 and type-2 rings, respectively. Thus, Fig. 2 unambiguously displays the same two types of rings previously described for the VCSEL model (Fig. 1).

IV. RINGS IN AN ELECTRONIC CIRCUIT

As a third complex oscillator, we consider the inductor-based Hartley oscillator, the dual of the more familiar capacitor-based Colpitts oscillator, both introduced in the 1910s, in the early days of transatlantic radiotelephone communications and which are still used in modern communication systems.[12,13]

Exceedingly complex oscillations generated by Hartley's oscillator are reported in several works.[36–40] Following experiments in Ref. 37, we consider Hartley's oscillator with a JFET and the usual

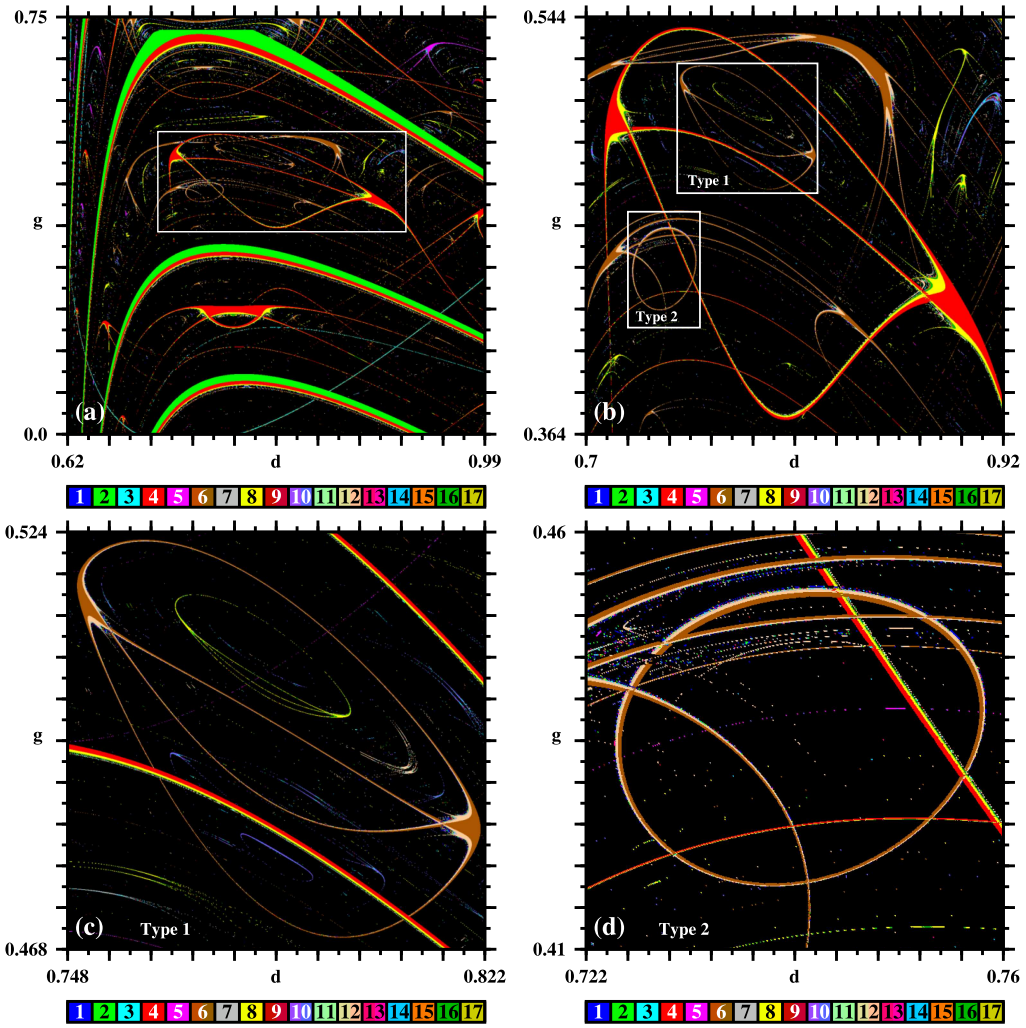

FIG. 2. Isospike stability diagrams showing type 1 and type 2 rings for the cells population model, Eq. (5), recorded in terms of the number of spikes per period of the active normal cells, N. (a) Main view, (b) magnification of the box in (a). Panels (c) and (d) are magnifications of the boxes in (b). Black marks chaotic oscillations, colors represent periodic oscillations, with the number of spikes per period shown by the colorbars. Note the profusion of many rather complex structures in these panels.

tapped coil.[38] Neglecting the internal resistance of the coil and using a high-frequency small-signal equivalent of the JFET, the equations governing the circuit are[37,38]

$$\begin{aligned} C_{GS}\frac{dv_{GS}}{dt} &= -i_1 + i_2 - i_D - i_d, \\ C_{GD}\frac{dv_{GD}}{dt} &= -i_2 + i_d, \\ L_1\frac{di_1}{dt} &= v_{GS}, \\ L_2\frac{di_2}{dt} &= -v_{GS} + v_{GD} + E, \end{aligned} \tag{6}$$

where $i_D = I_S\left[\exp\left(v_{GS}/V_T\right) - 1\right]$ and

$$i_d = \begin{cases} 0, & \text{if } v_{GS} \le V_c, \\ g(v_{GS} - V_c)^2, & \text{if } v_{GD} \le V_c, \\ g(v_{GS} - v_{GD})(v_{GS} + v_{GD} - 2V_c), & \text{if } v_{GD} \ge V_c. \end{cases}$$

Following previous works,[37,38] we fix $C_{GS} = 3.736\,\text{pF}$, $C_{GD} = 3.35\,\text{pF}$, $I_S = 33.57\,\text{fA}$, $V_c = -1.409\,\text{V}$, $V_T = 25\,\text{mV}$, $E = 2.8\,\text{V}$, $g = 1.754\,\text{mAV}^2$, $L_1 = 24.5\,\mu\text{H}$, and $L_2 = 4\,\mu\text{H}$ and classify oscillations for hundreds of millions of C_{GD} and L_2 values. As before, integrations were started from arbitrary initial conditions $(C_{GS}, C_{GD}, L_1, L_2) = (-1.25, -2.25, 10^{-6}, 10^{-6})$ but they are not critical. Using $h = 0.005$ as the timestep for integrations, we discarded

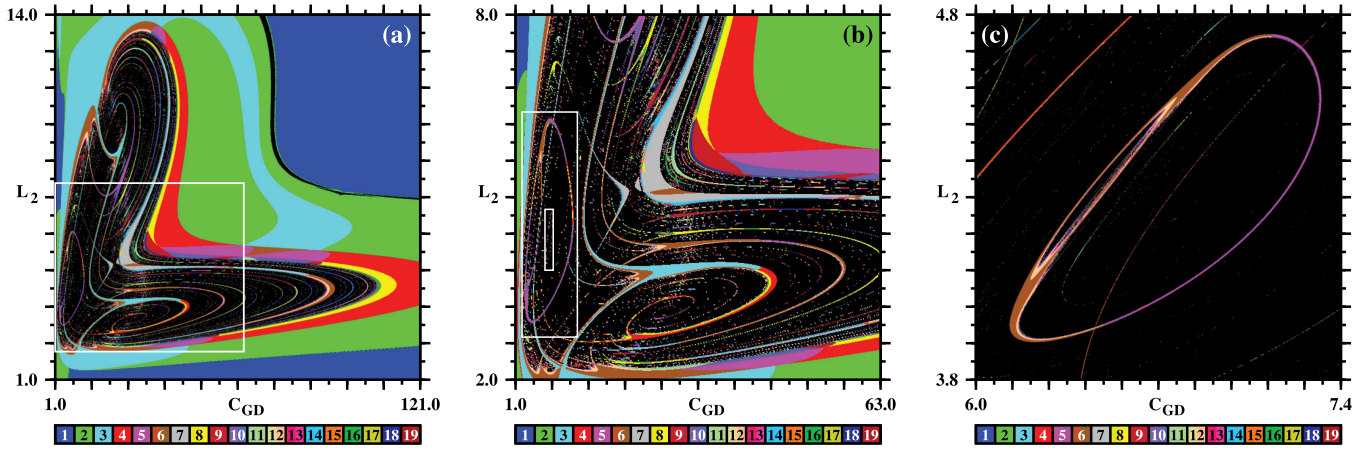

FIG. 3. Isospike stability diagrams illustrating rings and spirals[34] observed when counting spikes of v_{GD} for the JFET-based electronic circuit. (a) Large view of a control parameter plane. (b) Magnification of the box in (a) containing some rings. (c) Magnification of the smaller box in (b) showing a two-colors type-1 ring topologically similar to the larger ring seen in Fig. 1(b) for the VCSEL and in Fig. 2(c) for the model of cancerous cells subjected to radiation. Black represents parameters leading to chaotic oscillations and colors denote periodic oscillations, with the number of spikes per period encoded as indicated in the colorbars. Panels (a) and (b) contains several networks of *quint* points.[41]

transients of 85×10^6 steps, using an equal amount of steps to count spikes.

Figure 3(a) presents an isospike diagram for Hartley's oscillator focusing on the large region of abundant chaos, shown in black. The white box in this figure is shown magnified in Fig. 3(b), which contains two boxes with type-1 rings. The ring inside the smaller box is shown in Fig. 3(c). Type-2 rings also exist for Hartley's oscillator but are not shown here. Thus, once again, we find the same types of rings previously recorded for the VCSEL model (Fig. 1).

V. CONCLUSIONS

This paper reports the discovery of two types of stability rings, i.e., single or multiple closed loops, in the control parameter plane of a VCSEL. These rings are wide parameter circuits around which the laser may be tuned while preserving its wave pattern. From a practical point of view, rings are attractive because laser stability thrives along them, even in the presence of small parameter fluctuations. Our findings complement and extend certain aspects of previous works.[14–17] From a theoretical perspective, stability rings are interesting because there is no theory capable of predicting their existence and localization. Therefore, as done here, they must be sought by numerical analysis, something fortunately feasible nowadays with high-performance and high-throughput computer clusters working in parallel, benefiting from highly developed and reliable numerical methods. In addition to the VCSEL, rings were also not difficult to find in two additional and rather distinct applied systems, leading us to conjecture that the rings reported here are generic characteristics of large classes of dynamical systems. Within the framework of the three rate equation models used, we expect stability rings to be accessible to experimental verification, particularly, for the VCSEL and for Hartley's oscillator. We hope our findings will motivate their experimental observation as well as further applications.

ACKNOWLEDGMENTS

G.M.R.-A. acknowledges the German Academic Exchange Service for its support via the Re-invitation Program. J.K. was supported by the Russian Ministry of Science and Education (Agreement No. 075-15-2020-808). J.A.C.G. was partially supported by CNPq, Brazil, Grant No. 305305/2020-4. Bitmaps were computed on the PIK cluster, Potsdam, Germany, and the CESUP-UFRGS cluster of the Federal University in Porto Alegre, Brazil.

DATA AVAILABILITY

Data sharing is not applicable to this article as no new data were created or analyzed in this study.

REFERENCES

[1] J. Ohtsubo, *Semiconductor Lasers: Stability, Instability and Chaos*, 4th ed. (Springer, Berlin, 2017).
[2] P. W. Epperlein, *Semiconductor Laser Engineering, Reliability and Diagnostics* (Wiley, Chichester, 2013).
[3] in *Introduction to Nitride Semiconductor Blue Lasers and Light Emitting Diodes*, edited by S. Nakamura and S.F. Chichibu (Taylor and Francis, London, 2000).
[4] L. G. de Pillis and A. Radunskaya, "The dynamics of an optimally controlled tumor model: A case study," Math. Comput. Model. **37**, 1221–1244 (2003).
[5] M. R. Gallas, M. R. Gallas, and J. A. C. Gallas, "Distribution of chaos and periodic spikes in a three-cell population model of cancer," Eur. Phys. J.: Spec. Top. **233**, 2131–2144 (2014).
[6] R. Isea and K. Lonngren, "A mathematical model of cancer under radiotherapy," Int. J. Public Health Res. **3**, 340–344 (2015), http://www.openscienceonline.com/journal/archive2?journalId=718&paperId=2500.
[7] Z. Liu and C. Yang, "A mathematical model of cancer treatment by radiotherapy," Comput. Math. Methods Med. **2014**, 172923 (2014).
[8] R. P. Jiménez and E. O. Hernandez, "Tumour–host dynamics under radiotherapy," Chaos, Solitons Fractals **44**, 685–692 (2011).
[9] H. I. Freedman and G. Belostotski, "Perturbed models for cancer treatment by radiotherapy," Differ. Eqs. Dyn. Syst. **17**, 115–133 (2009).

[10]G. M. Ramírez-Ávila, "Estudio teórico de la acción de radiaciones ionizantes en la dinámica poblacional de células cancerosas," Rev. Boliviana Fis. **31**, 25–24 (2017), http://www.scielo.org.bo/pdf/rbf/v31n31/v31n31_a04.pdf.
[11]W. A. Canezo-Gómez, G. Rodrigo, and G. M. Ramírez-Ávila, "Análisis de la dinámica poblacional de células cancerosas, mediante un modelo de radiosensibilidad," Rev. Boliviana Fis. **35**, 5–14 (2019), http://www.scielo.org.bo/pdf/rbf/v35n35/v35n35_a02.pdf.
[12]U. Rohde and A. M. Apte, "Everything you always wanted to know about Colpitts oscillators," IEEE Microw. Mag. **17**, 59–76 (2016).
[13]U. Rohde, A. K. Poddar, and G. Böck, *The Design of Modern Microwave Oscillators for Wireless Applications* (Wiley, New York, 2005).
[14]I. Gatare, M. Sciamanna, J. Buesa, H. Thienpont, and K. Panajotov, "Nonlinear dynamics accompanying polarization switching in vertical-cavity surface-emitting lasers with orthogonal optical injection," Appl. Phys. Lett. **88**, 101106 (2006).
[15]M. Torre, A. Hurtado, A. Quirce, A. Valle, L. Pesquera, and M. J. Adams, "Polarization switching in long-wavelength VCSELs subject to orthogonal optical injection," IEEE J. Quantum Electron. **47**, 92–99 (2011).
[16]I. Gatare, M. Sciamanna, M. Nizette, H. Thienpont, and K. Panajotov, Phys. Rev. E **80**, 026218 (2009).
[17]H. Aoyama, S. Tomida, R. Shogenji, and J. Ohtsubo, "Chaos dynamics in vertical-cavity surface-emitting semiconductor lasers with polarization-selected optical feedback," Optics Commun. **284**, 1405–1411 (2011).
[18]A. Pikovsky and A. Politi, *Lyapunov Exponents, A Tool to Explore Complex Dynamics* (Cambridge University Press, Cambridge, 2016).
[19]J. G. Freire and J. A. C. Gallas, "Stern-Brocot trees in the periodicity of mixed-mode oscillations," Phys. Chem. Chem. Phys. **13**, 12191–12198 (2011).
[20]M. A. Nascimento, J. A. C. Gallas, and H. Varela, "Self-organized distribution of periodicity and chaos in an electrochemical oscillator," Phys. Chem. Chem. Phys. **13**, 441–446 (2011).
[21]J. G. Freire, T. Pöschel, and J. A. C. Gallas, "Stern-Brocot trees in spiking and bursting of sigmoidal maps," Europhys. Lett. **100**, 48002 (2012).
[22]J. A. C. Gallas, "Spiking systematics in some CO_2 laser models," Adv. Atom. Mol. Opt. Phys. **65**, 127–191 (2016).
[23]X. B. Rao, Y. D. Chu, L. Xu, Y. X. Chang, and J. G. Zhang, "Fractal structures in centrifugal flywheel governor system," Commun. Nonlin. Sci. Num. Simul. **50**, 330–339 (2017).
[24]L. Xu, Y. D. Chu, and Q. Yang, "Novel dynamical scenario of the two-stage Colpitts oscillator," Chaos, Solitons Fractals **138**, 109998 (2020).
[25]X. B. Rao, X. P. Zhao, J. S. Gao, and J. G. Zhang, "Self-organization with fast-slow time scale dynamics in a memristor-based Shinriki's circuit," Commun. Nonlin. Sci. Num. Simul. **94**, 105569 (2021).
[26]J. A. C. Gallas, M. J. B. Hauser, and L. F. Olsen, "Complexity of a peroxidase-oxidase reaction model," Phys. Chem. Chem. Phys. **23**, 1943–1955 (2021).
[27]J. A. C. Gallas, "Overlapping adding-doubling spikes cascades in a semiconductor laser proxy," Brazilian J. Phys. **51**, 919–926 (2021).
[28]J. A. Vélez, J. Bragard, L. M. Pérez, A. M. Cabanas, O. J. Suarez, D. Laroze, and H. L. Mancini, "Periodicity characterization of the nonlinear magnetization dynamics," Chaos **30**, 093112 (2020).
[29]C. S. Rodrigues, C. G. P. dos Santos, C. C. de Miranda, E. Parma, H. Varela, and R. Nagao, "A numerical investigation of the effect of external resistence and applied potential on the distribution of periodicity and chaos in the anodic dissolution of nickel," Phys. Chem. Chem. Phys. **22**, 21823–21834 (2020).
[30]J. A. C. Gallas, "Structure of the parameter space of the Hénon map," Phys. Rev. Lett. **70**, 2714–2717 (1993).
[31]J. A. C. Gallas, "Dissecting shrimps: Results for some one-dimensional physical systems," Physica. A. **202**, 196–223 (1994).
[32]Y. Zou, M. Thiel, M. C. Romano, and J. Kurths, "Shrimp structure and associated dynamics in parametrically excited oscillators," Int. J. Bif. Chaos **16**, 3567–3579 (2006).
[33]E. N. Lorenz, "Compound windows of the Hénon map," Physica D **237**, 1689–1704 (2008).
[34]C. Bonatto and J. A. C. Gallas, "Periodicity hub and nested spirals in the phase diagram of a simple resistive circuit," Phys. Rev. Lett. **101**, 054101 (2008).
[35]W. Façanha, B. Oldeman, and L. Glass, "Bifurcation structures in two-dimensional maps: The endoskeleton of shrimps," Phys. Lett. A **377**, 1264–1268 (2013).
[36]P. Kvarda, "Chaos in Hartley's oscillator," Int. J. Bifurcation Chaos **12**, 2229–2232 (2002).
[37]R. Tchitnga, H. B. Fotsin, B. Nana, P. H. L. Fotso, and P. Woafo, "Hartley's oscillator: The simplest chaotic two-component circuit," Chaos, Solitons Fractals **45**, 306–313 (2012).
[38]J. G. Freire and J. A. C. Gallas, "Cyclic organization of stable periodic and chaotic pulsations in Hartley's oscillator," Chaos, Solitons Fractals **59**, 129–134 (2014).
[39]M. Varan, A. Akgul, E. Guleryuz, and K. Serbest, "Synchronisation and circuit realisation of chaotic Hartley system," Z. Naturforschung A **73**, 521–531 (2018).
[40]A. Semenov, D. Havrilov, A. Volovik, S. Baraban, A. Savytskyi, and O. Zviahin, "Simulation of the chaotic dynamics of the deterministic chaos transistor oscillator based on the Hartley circuit," in *15th International Conference on Advanced Trends in Radioelectronics, Telecommunications and Computer Engineering* (IEEE, 2020).
[41]R. J. Field, J. G. Freire, and J. A. C. Gallas, "Quint points lattice in a driven Belousov-Zhabotinsky reaction model," Chaos **31**, 053124 (2021).